Bioactive Materials 27 (2023) 257–270

Contents lists available at ScienceDirect

Bioactive Materials

journal homepage: www.keaipublishing.com/en/journals/bioactive-materials

Novel neutrophil extracellular trap-related mechanisms in diabetic wounds inspire a promising treatment strategy with hypoxia-challenged small extracellular vesicles

Ziqiang Chu [a,b,1], Qilin Huang [c,1], Kui Ma [a,d,e,1], Xi Liu [a,d,e], Wenhua Zhang [a,d,e], Shengnan Cui [a,f], Qian Wei [a,b], Huanhuan Gao [a,b], Wenzhi Hu [a], Zihao Wang [a,b], Sheng Meng [a,b], Lige Tian [c], Haihong Li [g,*], Xiaobing Fu [a,b,c,d,e,f,**], Cuiping Zhang [a,d,e,***]

[a] Research Center for Tissue Repair and Regeneration Affiliated to the Medical Innovation Research Department, PLA General Hospital, 28 Fuxing Road, Beijing, 100853, PR China
[b] Chinese PLA Medical School, 28 Fuxing Road, Beijing, 100853, PR China
[c] College of Graduate, Tianjin Medical University, Tianjin, 300070, PR China
[d] Research Unit of Trauma Care, Tissue Repair and Regeneration, Chinese Academy of Medical Sciences, 2019RU051, 51 Fucheng Road, Beijing, 100048, PR China
[e] PLA Key Laboratory of Tissue Repair and Regenerative Medicine and Beijing Key Research Laboratory of Skin Injury, Repair and Regeneration, Chinese PLA Hospital and PLA Medical College, 51 Fucheng Road, Beijing, 100048, PR China
[f] Department of Dermatology, China Academy of Chinese Medical Science, Xiyuan Hospital, Beijing, 100091, PR China
[g] Department of Wound Repair, Institute of Wound Repair and Regeneration Medicine, Southern University of Science and Technology Hospital, Southern University of Science and Technology School of Medicine, Shenzhen, 518055, PR China

ARTICLE INFO

Keywords:
Diabetic wound healing
Neutrophil extracellular traps
Small extracellular vesicles
Hypoxia
Endoplasmic reticulum stress

ABSTRACT

Neutrophil extracellular traps (NETs) have been considered a significant unfavorable factor for wound healing in diabetes, but the mechanisms remain unclear. The therapeutic application of small extracellular vesicles (sEVs) derived from mesenchymal stem cells (MSCs) has received considerable attention for their properties. Hypoxic preconditioning is reported to enhance the therapeutic potential of MSC-derived sEVs in regenerative medicine. Therefore, the aim of this study is to illustrate the detailed mechanism of NETs in impairment of diabetic wound healing and develop a promising NET-targeting treatment based on hypoxic pretreated MSC-derived sEVs (Hypo-sEVs). Excessive NETs were found in diabetic wounds and in high glucose (HG)-induced neutrophils. Further research showed that high concentration of NETs impaired the function of fibroblasts through activating endoplasmic reticulum (ER) stress. Hypo-sEVs efficiently promoted diabetic wound healing and reduced the excessive NET formation by transferring miR-17–5p. Bioinformatic analysis and RNA interference experiment revealed that miR-17–5p in Hypo-sEVs obstructed the NET formation by targeting TLR4/ROS/MAPK pathway. Additionally, miR-17–5p overexpression decreased NET formation and overcame NET-induced impairment in fibroblasts, similar to the effects of Hypo-sEVs. Overall, we identify a previously unrecognized NET-related mechanism in diabetic wounds and provide a promising NET-targeting strategy for wound treatment.

Peer review under responsibility of KeAi Communications Co., Ltd.
* Corresponding author.
** Corresponding author. Research Center for Tissue Repair and Regeneration Affiliated to the Medical Innovation Research Department, PLA General Hospital, 28 Fuxing Road, Beijing, 100853, PR China.
*** Corresponding author. Research Center for Tissue Repair and Regeneration Affiliated to the Medical Innovation Research Department, PLA General Hospital, 28 Fuxing Road, Beijing, 100853, PR China.
E-mail addresses: lihaihong1051@126.com (H. Li), fuxiaobing@vip.sina.com (X. Fu), zcp666666@sohu.com (C. Zhang).
[1] These authors contributed equally to this work.

https://doi.org/10.1016/j.bioactmat.2023.04.007
Received 27 December 2022; Received in revised form 20 March 2023; Accepted 6 April 2023

1. Introduction

Diabetes is a sort of metabolic disorder diseases characterized by hyperglycemia [1]. Chronic non-healing wounds is one of the major complications of diabetes, accounting for 19–34% of diabetes patients [2]. Neutrophils, the most abundant type of circulating immune cells, are among the first to be recruited to the wound sites to participate in the early stage of wound healing [3]. The functions of neutrophils include phagocytosis, degranulation, and the formation of neutrophil extracellular traps (NETs). NETs were first described by Brinkmann in 2004 and regarded as framework that could bind and kill bacteria [4]. NETs are web-like structure composed of chromatin filaments decorated with granule proteins. During normal wound healing, low concentrations of NET could promote proliferation of epidermal keratinocytes [5]. Recently, excessive NET formation was found in diabetic wounds, suggesting a critical role of NETs in delayed wound healing [6]. However, little is known about the mechanisms responsible for the action of NETs on wound regeneration, and no NET-targeting treatment is currently approved for diabetic wound healing.

Currently, synthetic biomaterials, such as electrospinning [7] and hydrogels [8,9] were developed for diabetic wound healing. However, these materials lack the ability to modulate the wound microenvironments and cell behaviors around the wound. Recently, stem cells have been verified to promote wound healing and the performance of them after transplantation has increasingly been attributed to their exocrine function-producing derivatives such as small extracellular vesicles (sEVs) [10]. SEVs are nano-sized bilayer membrane structures carrying lipids, microRNAs (miRNAs), and proteins which act as therapeutic agents for the treatment of diseases. Compared with their parental cells, sEVs have many advantages including higher stability, absence of immune reactions, fewer ethical issues, and low possibility of embolism formation and carcinogenicity [11–13]. Additionally, sEVs display better histocompatibility, higher permeability, stronger biodegradability and lower cytotoxicity in comparison to those synthetic biomaterials [14,15]. At present, mesenchymal stem cells (MSCs) are the most common donor cells for sEVs. Recently, sEVs derived from human umbilical cord MSCs (hucMSCs) have received considerable attention for their use in cutaneous wounds [16]. Our latest research found that sEVs derived from hucMSCs could accelerate diabetic wound healing [17]. Although the role of sEVs in the development of many NET-associated diseases has been described [18–20], sEVs as therapeutic agents for treatment of NET-associated diseases have never been explored.

Current obstacles to the large-scale clinical applications of sEVs include low yield and inadequate therapeutic effect. Hypoxic preconditioning is reported not only to improve the yield of sEVs [21], but also to enhance the therapeutic effect of sEVs. For example, hypoxic pretreated adipose stem cell-derived sEVs were found to improve the healing of diabetic wounds via activating PI3K/AKT pathway in fibroblasts [22]. MiRNAs in sEVs are reported to be transferred into targeted cells, functioning by inhibiting the expression of their target genes. Moreover, several studies demonstrated that donor cells could respond to hypoxia by altering the molecular profile in sEVs. The miRNA profile in sEVs after hypoxic preconditioning has been investigated [23]. An exosomal miRNA analysis revealed that miR-17–5p was maximally enriched in sEVs derived from human bone marrow mesenchymal stem cells (BM-MSCs) challenged with hypoxia [24]. Furthermore, our previous study showed that miR-17–5p had the highest abundance in sEVs derived from hucMSCs cultured under normoxia [17]. However, the effect of hypoxia on the expression of miR-17–5p in hucMSC-sEVs has not been investigated, and whether hucMSC-derived sEVs miR-17–5p can regulate NET formation in diabetic wounds needs to be identified.

In this study, we first explored the NET-related mechanisms involved in impairment of diabetic wound healing and then identified Hypo-sEVs as a promising NET-targeting treatment. The results showed that excessive NET formation in neutrophils hindered diabetic wound healing via affecting the function of fibroblasts regulated by ER stress. Hypo-sEVs obstructed the excessive NET formation by transferring miR-17–5p to target TLR4/ROS/MAPK pathway, thereby enhancing the diabetic wound healing. Our work demonstrates a promising treatment strategy for the development of regenerative therapies for diabetic wound healing, and also provides potential for its application in treating NET-related diseases.

2. Materials and methods

2.1. Cell lines

The hucMSCs and human fibroblasts were purchased from the Chinese Academy of Sciences' cell bank and maintained in Dulbecco's modified Eagle's medium/F12 (DMEM/F12, Gibco, USA) supplemented with 10% fetal bovine serum (FBS, Gibco, USA) at 37 °C with 5% CO_2. The concentration of glucose to induce high glucose (HG)-fibroblasts is 35 mM and the treatment lasted for 2 months.

2.2. Normoxia and hypoxia preconditioning protocols

MSCs were cultured to 70% confluence and then cultured under ambient atmospheric conditions of 21% O_2 and 5% CO_2 (normoxia) or in a hypoxic incubator with 1% O_2 (hypoxia) at 37 °C for 48 h.

2.3. SEVs isolation and characterization

The isolation of sEVs from MSCs was performed by ultracentrifugation as described previously [22]. Briefly, after 2–3 passages, when the cell reached 70% confluence, the complete culture medium of MSCs was replaced with DMEM/F12 containing 10% sEV-depleted FBS (SBI, USA). Forty-eight hours later, the culture medium was collected, centrifuged at 2000×*g* for 10 min and 10,000×*g* for 30 min at 4 °C to remove dead cells, cellular debris and apoptotic bodies. Then the supernatants were passed through a 0.22 μm membrane filters (Millipore, SLGP033RB) and centrifuged at 100,000×*g* for 75 min. Subsequently, the supernatants were discarded, and the pellet was resuspended in phosphate-buffered saline (PBS). The resuspensions were centrifuged again at 100,000×*g* for 75 min, and the deposition was resuspended with PBS for following application or stored at −80 °C.

Nanoparticle tracking analyzer (NTA) (Particle Metrix GmbH, Germany) and transmission electron microscope (TEM) (Hitachi, Japan) were used to measure the particle size and concentration of sEVs. Expression of the sEVs markers was determined by Western blot, including CD63, CD9, tumor susceptibility gene 101 (TSG101) and Calnexin.

2.4. Uptake of sEVs

Dil solution (Molecular Probes, Eugene, OR, USA) was applied to label sEVs fluorescently to track internalization according to the manufacturer's protocol. In short, we incubated sEVs (2×10^9 particles mL^{-1}) with Dil solution for 15 min at room temperature. The labeled sEVs were centrifuged at 100,000×*g* for 75 min at 4 °C and then resuspended with PBS. Next, neutrophils and Dil-labeled sEVs were co-cultured for 12 h at 37 °C, then the cells were washed with PBS and fixed with 4% paraformaldehyde. Nuclei was stained with DAPI (Thermo Fisher, USA) for 10 min. The image was observed by a laser confocal microscopy (Leica, Germany).

2.5. Human neutrophil isolation

Human neutrophils were isolated from peripheral blood of healthy donors by using human peripheral blood neutrophil separation kit (TianJinHaoYang Biological Manufacture Co.). May-Grunwald-Giemsa staining (40751ES02, Yeasen) was used to determine the purity of the isolated neutrophils. Neutrophils were cultured in RPMI-1640 medium

(Gibco, Shanghai, China) with 10% FBS at 37 °C with 5% CO_2.

2.6. In vitro NET analysis

Neutrophils (2×10^5 cells) attached on coverslips coated with poly-L-lysine (P4707, Sigma) in 24-well plates were preincubated with or without sEVs (2×10^9 particles mL^{-1}) for 24 h at 37 °C. After that, the neutrophils were stimulated with 20 nM PMA (Sigma) or different concentrations of glucose for 3 h. Next, neutrophils were fixed with 4% paraformaldehyde for 30 min at room temperature. Then neutrophils were washed with PBS and permeabilized with 0.2% Triton X-100 for 10 min. Subsequently, cells were blocked in PBS with 5% BSA for 30 min at room temperature and then incubated with citrullinated histone H3 (H3Cit, 1:200, Abcam, ab5103) and myeloperoxidase (MPO, 10 μg mL^{-1}, R&D, AF3667) in blocking buffer overnight at 4 °C. After washing with PBS, cells were incubated with Alexa-Fluor-conjugated secondary antibodies (A21206, A21447; Invitrogen) for 1 h at room temperature. DAPI (Thermo Fisher, USA) was used to counterstain the nuclei for confocal laser scanning microscopy. The NETs areas were analyzed as the percentage of the positive H3Cit signal areas divided by total DNA areas in each field by using Imaris Microscopy Image Analysis software.

2.7. Purification of NETs

NETs were isolated from human neutrophils according to a previous reported method [25]. In brief, neutrophils were incubated with PMA (500 nM) for 4 h at 37 °C. After discarding of supernatant, NETs adhered to the bottom of plate were resuspended with cold D-PBS (without calcium, magnesium and phenol red). The resuspensions were centrifuged at 450×*g* for 10 min and the supernatants containing NETs were collected. After centrifugation at 18,000×*g* for 10 min at 4 °C, the deposition (NETs) was resuspended with D-PBS for further study or stored at −80 °C. The DNA concentration of NETs was calculated by spectrophotometry.

2.8. MiRNA/siRNA transfection

Small interfering RNAs (TLR4 siRNAs), miR-17–5p mimics, and miR-17–5p inhibitors as well as their corresponding control oligonucleotides were purchased from GenePharma. Transfection was carried out by using Lipofectamine 2000 reagent (Invitrogen) based on the manufacturer's instructions. The oligonucleotide sequences of TLR4 siRNAs are listed in Table S1. Then the cells were collected for further study.

2.9. Lentivirus vector constructs and transfection

Lentiviral vectors containing miR-17–5p mimic (miR-17^{OE}), miR-17–5p inhibitor (miR-17^{KD}) as well as their corresponding negative control were purchased from GenePharma.

2.10. RNA isolation and RT-qPCR

Total RNA was isolated via using TRIzol reagent (Takara, Japan) according to the manufacturer's protocol. Reverse transcription was performed by application of PrimeScript RT Reagent Kit (Takara, Japan) and miRNA RT Reagent kit (Accurate Biology, China). Real-time PCR was performed with Accurate Taq PCR reagent kit (Accurate Biology, China) on an ABIPRISMVR 7300 Sequence Detection System (Applied Biosystems). The specific primers are listed in Table S2.

2.11. Luciferase reporter assay

The binding site between miRNAs and target genes was examined by the use of dual-luciferase reporter assay as previously described [26]. Briefly, PsiCHECK2 (IGE Biotech, China) vector included firefly luciferase gene (hLuc+) and renilla luciferase gene (hRluc) was used in this assay. Luciferase reporter assay was performed to explore whether TLR4 was the direct target of miR-17–5p. The 3′ UTR sequence of TLR4 was cloned into the vectors (PsiCHECK2-WT-TLR4 and PsiCHECK2-MUT-TLR4). According to the manufacturer's instructions, TLR4 vector was co-transfected with NC or miR-17–5p mimics. The relative value of luciferase was measured by Centro LB960 XS3 (Berthold, German).

2.12. NETs stimulation

Fibroblasts were preincubated with or without ER stress inhibitor (4-phenylbutyrate, 4-PBA, 5 μM, HY-A0281, MedChem Express) for 1.5 h. Subsequently, different concentrations of NETs were added into the supernatant for 24 h at 37 °C. For degradation of NETs, the culture media contained NETs was treated with DNase I (2 U mL^{-1}, 89836, ThermoFisher Scientific) for 1 h at 37 °C.

2.13. Immunoblotting

Cells were collected and lysed with RIPA buffer containing proteinase inhibitor. The protein concentration was measured with BCA method (Solarbio, China). Proteins were separated on SDS-PAGE and electro-transferred to nitrocellulose membranes (Millipore). After blockage, the membranes were incubated at 4 °C overnight with primary antibodies including CD63 (1:1000, ProteinTech, 25682-1-AP), CD9 (1:1000, ProteinTech, 20597-1-AP), TSG101 (1:1000, ProteinTech, 28283-1-AP), Calnexin (1:1000, ProteinTech, 10427-1-AP), TLR4 (1:1000, ProteinTech, 19811-1-AP), p-ERK (1:1000, CST, 4370), p-JNK (1:1000, CST, 4668), p-p38 (1:1000, CST, 4511), PERK (1:1000, CST, 5683), p-PERK (1:1000, CST, 3179), EIF2α (1:1000, ProteinTech, 11170-1-AP), p- EIF2α (1:1000, ProteinTech, 28740-1-AP), ATF4 (1:1000, ProteinTech, 10835-1-AP), CHOP (1:1000, CST, 2895), Caspase 12 (1:1000, ProteinTech, 55238-1-AP), cleaved caspase 3 (1:1000, Abcam, ab32042) or β-actin (1:1000, Abcam, ab8226). Peroxidase-conjugated (HRP)-linked secondary antibody (CST) was used to incubate with these membranes for 1 h at room temperature. The antigen–antibody reaction was visualized via an ECL kit (ECL, Thermo) and imaged by UVITEC Alliance MINI HD9 system (UVITEC, Britain).

2.14. Edu assay

Fibroblasts were seeded in 24-well plates and cultured for 24 h before the administration of Edu assay kit (Beyotime Biotechnology, China). Subsequently, cells were fixed, permeabilized and stained according to the manufacturer's instructions. Images and analysis were acquired by using a fluorescence microscope.

2.15. Cell counting kit-8 proliferation assay

Cells' proliferation ability was measured by cell counting kit-8 (CCK8) assay (APExBIO, Houston, USA). Cells (1000 cells per well) in the logarithmic growth phase were seeded into 96-well plates and CCK8 (10 μL per well) solution was added into the medium (100 μL per well), followed by an incubation at 37 °C for 2 h. The absorbance was spectrophotometrically measured at the wavelength of 450 nm for 3 times by an enzyme immunoassay analyzer (Bio-Rad 680, Hercules, USA).

2.16. Cell migration assay

Scratch and transwell assay were used to evaluate the migration ability of fibroblasts. For scratch assay, fibroblasts were seeded into 6-well plates and cultured to 90% confluence. Then the cells were scratched with a pipette tip. Images of the cells were obtained at 0, 12 and 24 h via a microscope. Migration areas was measured by ImageJ software. For transwell assay, cell suspensions (1×10^4 cells) were diluted in 0.2 mL of serum-free medium and seeded into the upper

chamber of 24-well plates with 8.0 μm polycarbonate membrane (Corning). Lower chambers were added with complete medium. After 24 h, upper membrane cells were removed and the migrated cells on the lower surface were stained with crystal violet (Beyotime, China). After washing with PBS, the stained cells were counted through an optical microscope.

2.17. Measurement of ROS production

To measure the level of ROS in each group, according to the manufacturer's instructions, neutrophils pretreated with or without stimulations were incubated with 10 μM DCFH-DA (Beyotime Biotechnology, China) at 37 °C for 20 min, then washed with PBS and re-suspended in 200 μL PBS for detection. Total ROS production was measured by fluorescence spectrophotometer and visualized by fluorescence microscope (Nikon Eclipse 80i, Japan).

2.18. Animals

Eight-weeks-old male (BKS-Dock Lepr^{em2Cd479}, db/db) diabetic mice were purchased from SPF (Beijing, China) Biotechnology Co., Ltd. and used for diabetic wound healing evaluation. The animal studies were approved by the Animal Research Committee of PLA General Hospital in Beijing, China. All mice were fed under standard laboratory condition free of specific pathogens. Full-thickness skin wounds with a diameter of 10 mm were produced on the back of each mouse. Then all mice were randomly divided into sEVs groups and control groups (n = 6). PBS (100 μL), Normo-sEVs (100 μL, 2×10^{10} particles mL^{-1}), Hypo-sEVs (100 μL, 2×10^{10} particles mL^{-1}), miR-NC^{OE}-sEVs (100 μL, 2×10^{10} particles mL^{-1}), miR-17^{OE}-sEVs (100 μL, 2×10^{10} particles mL^{-1}), miR-NC^{KD}-sEVs (100 μL, 2×10^{10} particles mL^{-1}) or miR-17^{KD}-sEVs (100 μL, 2×10^{10} particles mL^{-1}) were subcutaneously injected around the wounds at 4 sites (25 μL per site) every other day. The wounds were photographed and analyzed by Image J software on days 0, 3, 7 and 14 after the wound operation respectively. The mice were euthanized by using 10% chloral hydrate. The healing wound tissues and surrounding areas were harvested on days 3, 7 and 14 for further study.

2.19. Histological examination

The obtained wound tissues were fixed with 4% paraformaldehyde for at least 24 h, then dehydrated through a graded series of ethanol and embedded in paraffin. The embedded tissues were sectioned to 5 μm thick sections, subsequently hematoxylin and eosin (H&E) and Masson's trichrome staining were conducted. The histological images were analyzed as described previously [17,27].

2.20. Immunofluorescence

The sections of wound tissues were deparaffinized, rehydrated and antigen retrieved. After blockage, the sections were incubated with primary antibodies against H3Cit (1:200, Abcam, ab5103) and MPO (10 μg mL^{-1}, R&D, AF3667) in blocking buffer overnight at 4 °C, followed by incubation with Alexa-Fluor-conjugated secondary antibodies (A21206, A21447; Invitrogen) for 1 h at room temperature. DAPI (Thermo Fisher, USA) was used to counterstain the nuclei for confocal laser scanning microscopy. H3Cit^{+} areas in each field of view in the wound edges were identified as NETs areas in tissues.

2.21. Statistical analysis

All the results in this study were shown as the mean ± standard deviation of at least three independent experiments. The differences among multiple groups were evaluated with analysis of one-way variance (ANOVA) or Student *t*-test, where appropriate. *P* values < 0.05 was considered to be statistically significant. Statistical analyses were performed with GraphPad Prism 8.0 and R 4.2.1.

3. Results

3.1. Excessive NET formation hinders diabetic wound healing by affecting fibroblast function

To confirm the excessive formation of NETs in diabetic wounds, we created full-thickness cutaneous wounds on the backs of diabetic mice. Citrullinated histone H3 (H3Cit) and myeloperoxidase (MPO) were used as the specific markers for NETs and neutrophils, respectively [28]. As expected, higher production of NETs with neutrophil infiltration was observed in diabetic wounds compared with normal wounds (Fig. 1a). To further confirm that NET formation was caused by hyperglycemia, we extracted neutrophils from peripheral blood of healthy volunteers and identified them with Giemsa staining (Supplementary Fig. S1). Subsequently, neutrophils were treated with glucose at concentrations of 5.5, 15, 25, and 35 mM. NETs extension was evaluated by immunofluorescence staining and we observed that high concentration of glucose could prime neutrophils to produce NETs (a process termed NETosis) in a dose-dependent manner (Fig. 1b, d). Moreover, NET-inducer phorbol-12-myristate-13-acetate (PMA) [29] was used as a positive control (Fig. 1c, e).

Although the negative effect of NETs in diabetic wound healing has been reported, the cellular mechanisms responsible for the effect of NETs remain undetermined. It's well known that fibroblasts are crucial for supporting wound healing. We next investigated the effect of NETs on the function of fibroblasts. NETs were extracted from neutrophils treated with PMA for further study. Fibroblasts induced by high glucose (HG) were treated with different concentrations of NETs (0 ng mL^{-1}, 100 ng mL^{-1}, and 1000 ng mL^{-1}) for 24 h. The results of Edu and CCK8 assays showed that low concentration of NETs (100 ng mL^{-1}) significantly increased the proliferation of fibroblasts, while fibroblasts treated with high concentration of NETs (1000 ng mL^{-1}) exhibited lower proliferation ability (Fig. 1f–h). Moreover, scratch and transwell assays were used to assess the migration ability of fibroblasts. Similarly, NETs promoted fibroblast migration in the low concentration group and opposite effects were found in the high concentration group (Fig. 1i-l). These findings suggest that excessive NET formation in diabetic wounds inhibits the wound healing via impairing the function of fibroblasts, although low concentration of NETs displays an opposite effect.

3.2. ER stress is responsible for impairment of fibroblast function induced by excessive NETs

Sustained endoplasmic reticulum (ER) stress can initiate apoptosis of cells. A previous study reported that NETs could impair intestinal barrier functions in sepsis via activating ER stress which could finally induce intestinal epithelial cell death [30]. Another research revealed that NETs contributed to acute lung injury by directly driving ER stress in alveolar epithelial cells [31]. However, whether ER stress is responsible for NET-induced impairment on fibroblast function remains unclear. Fibroblasts were treated with a dilution series of NETs (from 0 to 1000 ng mL^{-1}) isolated from PMA-induced neutrophils for 24 h. The biomarkers of ER stress including p-PERK, p-EIF2α, ATF4, and CHOP were detected by Western blot. The results demonstrated that the expressions of these markers were increased by NETs in a dose-dependent manner (from 200 to 1000 ng mL^{-1}), except for low concentration of NETs (100 ng mL^{-1}). Moreover, the biomarkers of apoptosis including caspase 12 and cleaved caspase 3 had the same performance (Fig. 2a). Next, 4-PBA (inhibitor of ER stress) or DNase I which could degrade NET-DNA [6] was used before stimulating fibroblasts with high concentration of NETs (1000 ng mL^{-1}). Expectedly, we found that the expressions of biomarkers of ER stress and apoptosis in fibroblasts decreased to normal level after administration of 4-PBA or DNase I (Fig. 2b). Meanwhile, the application of 4-PBA or DNase I also abolished the unfavorable effect of NETs on proliferation

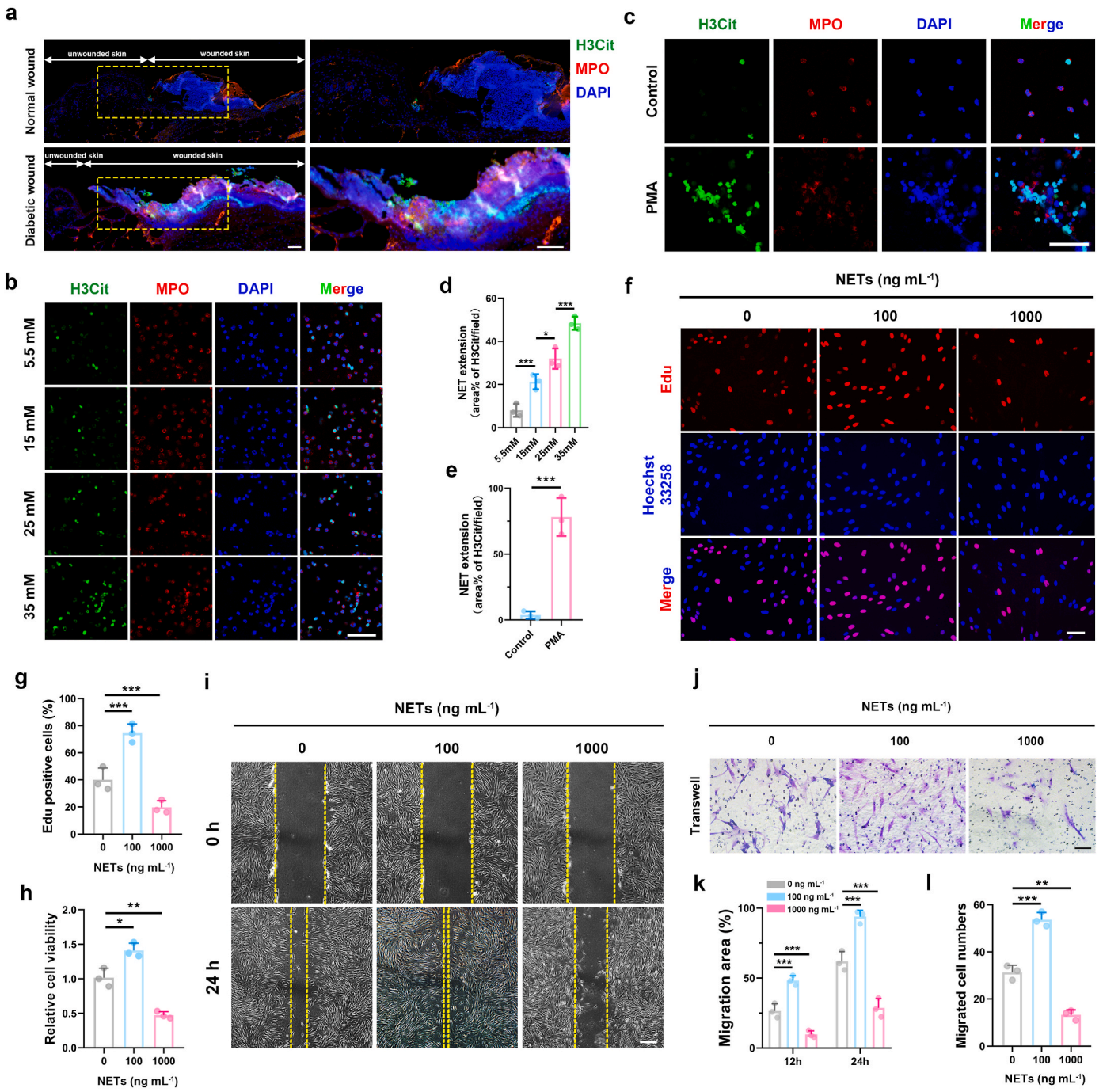

Fig. 1. Excessive NET formation hinders diabetic wound healing by affecting fibroblast function. (**a**) Representative confocal images of wounds in normal and diabetic mice at 3 days after injury. Areas enclosed by the yellow box is magnified and shown on the right. H3Cit, Green; MPO, red; DAPI, blue. Scale bar, 100 μm. (**b-e**) After stimulating by different concentrations of glucose or PMA (20 nM) for 3 h, NET formation was observed and quantified through immunofluorescence. H3Cit, Green; MPO, red; DAPI, blue. Scale bar, 50 μm. (**f-h**) Edu and CCK8 assays were performed to evaluate proliferation of high-glucose-induced fibroblasts treated with or without NETs at low (100 ng mL^{-1}) or high (1000 ng mL^{-1}) concentration. Edu, red; DAPI, blue. Scale bar, 50 μm. (**i, k**) Migration ability of fibroblasts in different groups was measured by wound scratch assay. Scale bar, 100 μm. (**j, l**) Migration ability of fibroblasts in different groups was measured by transwell assay. Scale bar, 50 μm $^{*}p < 0.05$, $^{**}p < 0.01$, $^{***}p < 0.001$.

(Fig. 2c–e) and migration (Fig. 2f–i) abilities of fibroblasts. These results suggest that excessive production of NETs impairs fibroblast function via driving ER stress.

3.3. *Hypoxia-induced sEVs accelerate diabetic wound healing by reducing excessive NET formation in vivo*

Recent studies suggest that hypoxia-induced sEVs (Hypo-sEVs) have better performance than normoxia-induced sEVs (Normo-sEVs) on treating diseases. In this study, Normo-sEVs and Hypo-sEVs were obtained from hucMSCs which had been used in our preliminary research [17]. To identify the characters of sEVs, nanoparticle tracking analysis (NTA), transmission electron microscope (TEM) and Western blot were applied. NTA and TEM showed that both Normo-sEVs and Hypo-sEVs had similar diameter size distribution (average 123.4 nm VS 121.8 nm) and "saucer-like" ultrastructure (Fig. 3a and b). Representative

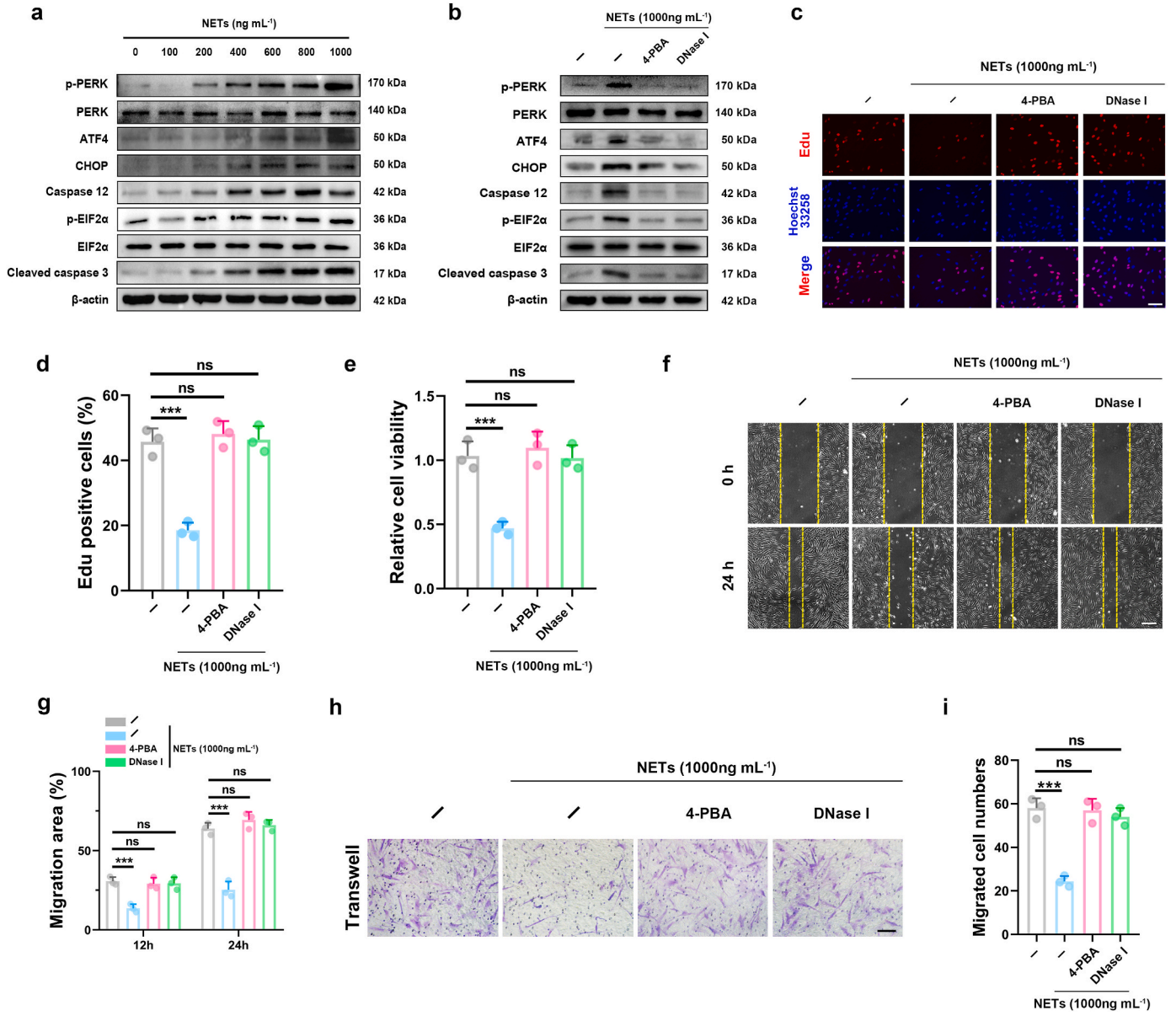

Fig. 2. ER stress is responsible for impairment of fibroblast function by excessive NETs. (**a**) Immunoblotting of ER stress and apoptosis markers in HG-induced fibroblasts. NETs at increasing concentrations (0–1000 ng mL^{-1}) were added into the culture media and incubated for 24 h. (**b**) The protein levels of key molecules of ER stress and apoptosis in HG-induced fibroblasts after NET (1000 ng mL^{-1}) treatment with or without pre-incubation with 4-PBA (5 μM) or DNase I (2 U mL^{-1}). (**c-e**) Edu and CCK8 assays were performed to evaluate proliferation of HG-induced fibroblasts following the indicated treatment with 4-PBA (5 μM) or DNase I (2 U mL^{-1}). Edu, red; DAPI, blue. Scale bar, 50 μm. (**f, g**) Migration ability of HG-induced fibroblasts was analyzed by wound scratch assay following the indicated treatment with 4-PBA (5 μM) or DNase I (2 U mL^{-1}). Scale bar, 100 μm. (**h, i**) Migration ability of HG-induced fibroblasts was analyzed by transwell migration assay following the indicated treatment with 4-PBA (5 μM) or DNase I (2 U mL^{-1}). Scale bar, 50 μm. ns: no significance, $^{***}p < 0.001$.

surface markers of sEVs including CD63, CD9 and TSG101 were expressed in sEVs groups, while Calnexin expression was only detected in cell lysis group (Fig. 3c). Collectively, these results indicate that the isolated nanoparticles are sEVs. To further confirm that Hypo-sEVs might have better effect on improving diabetic wound healing than Normo-sEVs. Full-thickness cutaneous wounds were created and then treated with PBS, Normo-sEVs or Hypo-sEVs by intradermally injection at the wound edge every other day. Compared to control (PBS) group, the rate of wound healing was significantly faster following the administration of either Normo-sEVs or Hypo-sEVs. As expected, Hypo-sEVs infusion resulted in better improvement of wound healing compared with the Normo-sEVs group (Fig. 3d–f). Then H&E staining was performed to evaluate the wound length in each group and the tendency was consistent with the aforementioned dimensions of wound areas (Fig. 3g and h). Furthermore, we also observed the effect of Hypo-sEVs on the excessive NET formation in diabetic wounds. Notably, the over-produced NETs were observed in the control group and administration of Normo-sEVs or Hypo-sEVs significantly reduced the NET accumulation in diabetic wounds. In addition, Hypo-sEVs played a more effective role in reducing NET formation (Fig. 3i). Moreover, Masson staining showed that wounds treated with Hypo-sEVs had more extensive collagen deposition than that in the Normo-sEVs group and control group, and downregulation of CHOP protein level, biomarker of ER stress, was observed in vimentin $^{+}$ dermal fibroblasts (Supplementary Figs. S2a and b). Together, these data imply that both Normo-sEVs and Hypo-sEVs can accelerate diabetic wound healing via inhibiting NET formation and NET-induced ER stress, and the effects of Hypo-sEVs are more obvious than Normo-sEVs.

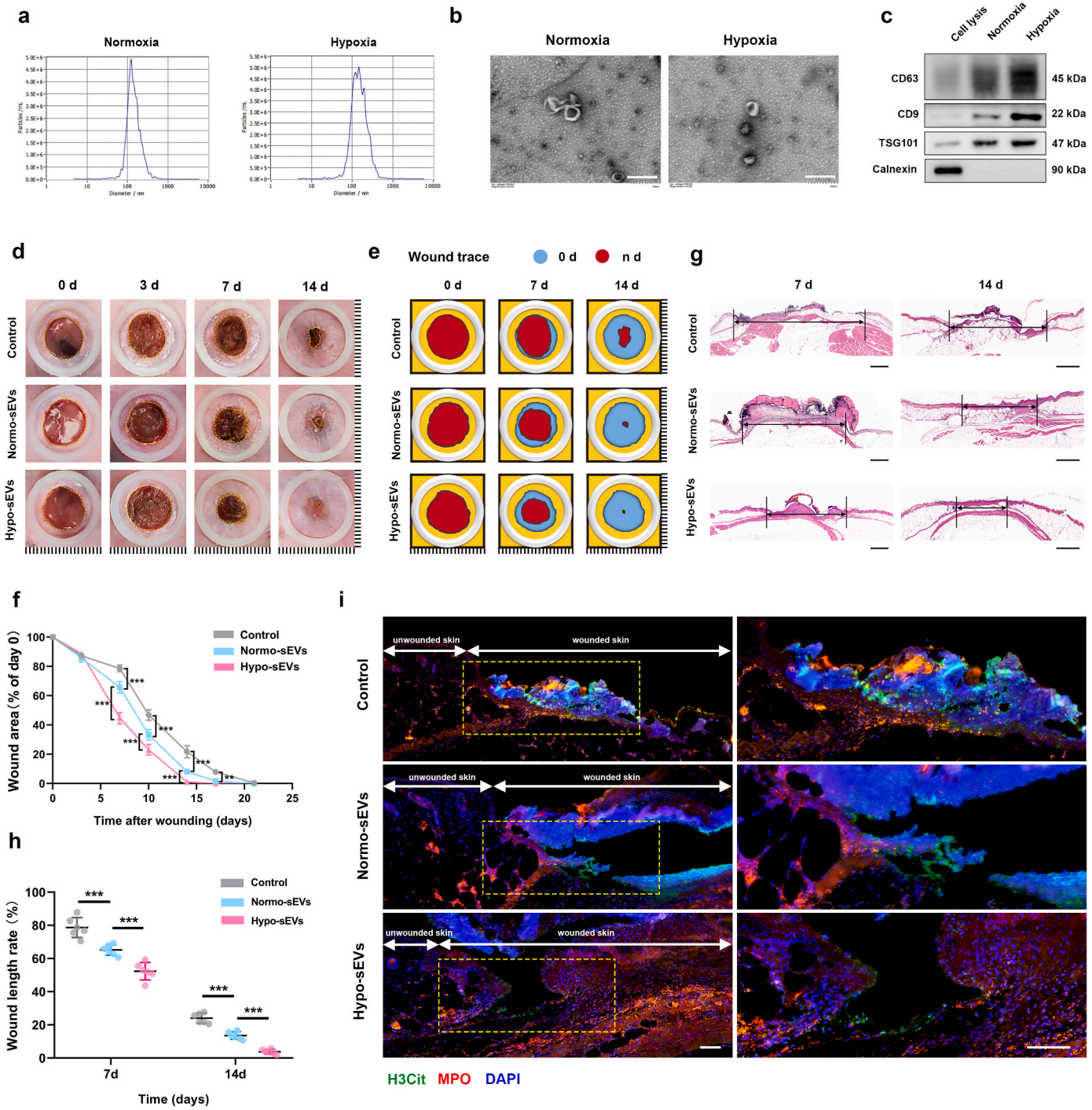

Fig. 3. Hypoxia-induced sEVs accelerate diabetic wound healing by reducing excessive NET formation in vivo. (**a**) The size distribution and concentration of MSC-derived Normo-sEVs and Hypo-sEVs were measured by NTA. (**b**) Representative TEM photomicrographs of Normo-sEVs and Hypo-sEVs. Scale bars, 200 nm. (**c**) The expression of sEVs markers including CD63, CD9, TSG101 and Calnexin was determined by Western blot. (**d**) Gross view of diabetic wounds on days 0, 3, 7 and 14 post wounding with the administration of PBS, Normo-sEVs or Hypo-sEVs. (**e**) Simulation plots of the wound closure areas. (**f**) Quantitative evaluation of the wound closure rate; n = 6. (**g**) Representative images of H&E staining of wound sections. Scale bar, 2 mm. (**h**) Quantitative analysis of the wound length rate; n = 6. (**i**) Immunofluorescence analysis of NETs areas in diabetic wounds on day 3 post wounding with the administration of PBS, Normo-sEVs or Hypo-sEVs. H3Cit, Green; MPO, red; DAPI, blue; n = 6. Scale bar, 100 μm $^{**}p < 0.01$, $^{***}p < 0.001$.

3.4. Hypoxia-induced sEVs transferring miR-17–5p obstruct the NET formation by downregulating TLR4/ROS/MAPK pathway in vitro

To further investigate the mechanism of Hypo-sEVs on NET formation, a series of in vitro experiments on neutrophils were performed. Normo-sEVs and Hypo-sEVs were labeled with Dil dye and then incubated with neutrophils for 24 h. We observed that Normo-sEVs and Hypo-sEVs were able to be taken up by neutrophils (Fig. 4a). After administration of PMA (20 nM) or high concentration of glucose (35 mM), NETosis was found to be less in Normo-sEVs and Hypo-sEVs groups. Furthermore, the ability of Hypo-sEVs to reduce the NETs areas was more powerful than that of Normo-sEVs (Fig. 4b). Our recent study confirmed that miR-17–5p could improve diabetic wound healing through enhancement of angiogenesis and miR-17–5p was the most

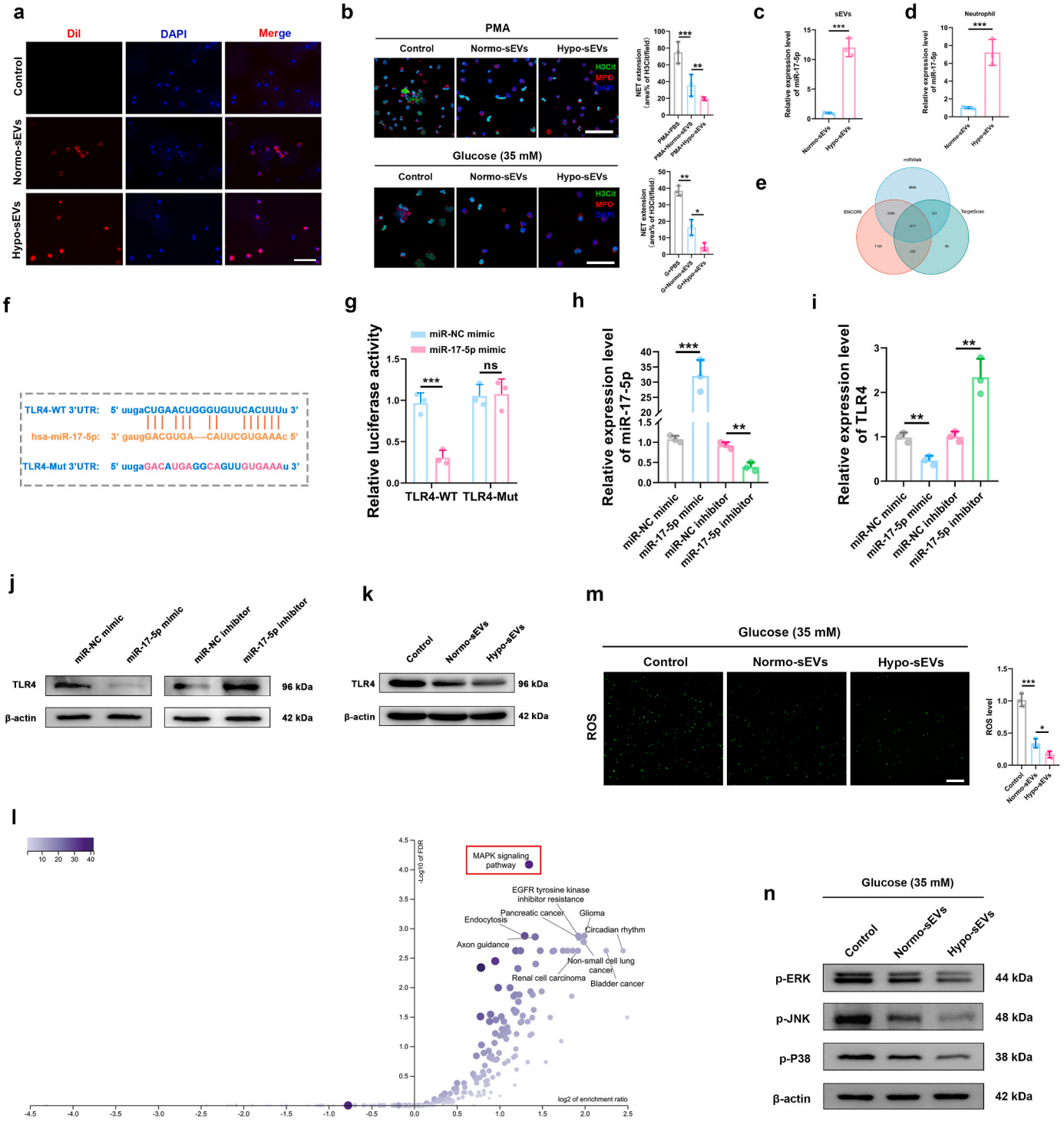

Fig. 4. Hypoxia-induced sEVs transferring miR-17–5p obstruct the NET formation by downregulating TLR4/ROS/MAPK pathway in vitro. (**a**) Uptake of Dil-labeled sEVs into neutrophils. Dil, red; DAPI, blue. Scale bar, 50 μm. (**b**) Representative immunofluorescence images of H3Cit, MPO and DAPI staining of neutrophils incubated with or without sEVs for 24 h in the presence of PMA (20 nM) or high concentration of glucose (35 mM). H3Cit, Green; MPO, red; DAPI, blue. Scale bar, 50 μm. (**c**) Expression level of miR-17–5p in Normo-sEVs and Hypo-sEVs was measured by RT-qPCR. (**d**) Expression level of miR-17–5p in neutrophils, measured by RT-qPCR, after incubation with Normo-sEVs or Hypo-sEVs for 24 h. (**e**) Target genes of miR-17–5p were predicted by using ENCORI, miRWalk and TargetScan database. According to the Venn diagram, 917 genes were screened out by using R software. (**f**) Predicted binding site between miR-17–5p and TLR4. (**g**) Interaction between miR-17–5p and TLR4 was confirmed by luciferase reporter assay. (**h**) Expression level of miR-17–5p in neutrophils after transfection of miR-17–5p mimic or inhibitor assayed by RT-qPCR. (**i**) TLR4 mRNA expression level in neutrophils after transfection of miR-17–5p mimic or inhibitor assayed by RT-qPCR. (**j**) TLR4 protein expression level in neutrophils after transfection of miR-17–5p mimic or inhibitor measured by Western blot. (**k**) Western blot analysis of TLR4 protein expression level in neutrophils after administration of Normo-sEVs or Hypo-sEVs. (**l**) KEGG pathway analysis showed that MAPK signaling pathway was involved in the downstream of miR-17–5p. (**m**) ROS generation in neutrophils was performed by using DCFH-DA after incubation with or without sEVs. Scale bar, 200 μm. (**n**) The protein level of p-ERK, p-JNK and p-p38 were detected in different groups by Western blot. $^{*}p < 0.05$, $^{**}p < 0.01$, $^{***}p < 0.001$.

abundant miRNA in Normo-sEVs according to a miRNA microarray [17]. Additionally, miR-17–5p expression in sEVs derived from bone marrow mesenchymal stem cells (BM-MSCs) can be enhanced by hypoxic precondition [24]. In our study, we also observed a higher expression level of miR-17–5p in Hypo-sEVs (Fig. 4c) and in neutrophils treated with Hypo-sEVs (Fig. 4d). These results indicated that Hypo-sEVs can transport more miR-17–5p into neutrophils.

To address the mechanism of Hypo-sEVs miR-17–5p in NETosis, we predicted the target genes of miR-17–5p by using ENCORI, miRWalk and TargetScan database. According to the Venn diagram, we screened out 917 genes by using R software (Fig. 4e). Combined with the bioinformatic analysis and literature study, TLR4 was predicted as a target of miR-17–5p (Fig. 4f). To further confirm this hypothesis, luciferase assay was applied to identify the interaction between miR-17–5p and TLR4. Wild-type (WT) or mutant (Mut) 3′ UTR sequences of TLR4 based on the potential binding sites was cloned into the luciferase reporter plasmid and co-transfected with miR-17–5p mimic or miR-NC mimic into 293T cells. The result showed that miR-17–5p overexpression significantly suppressed the luciferase reporter activity of the vector including the WT binding site but not the mutant binding site (Fig. 4g). Next, RT-qPCR was performed to confirm the transfection efficiency of miR-17–5p mimic and inhibitor in neutrophils (Fig. 4h).

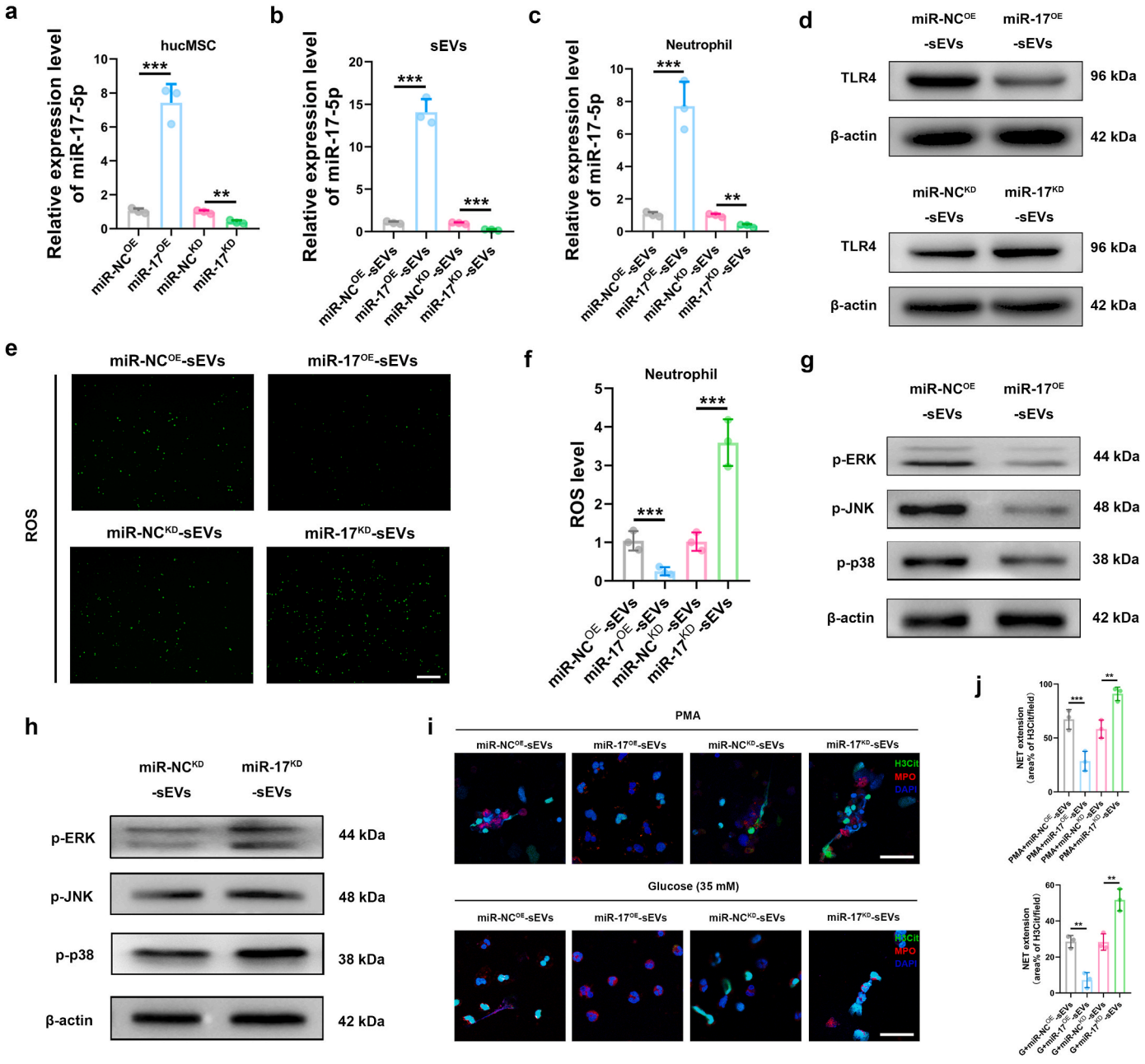

Fig. 5. MiR-17–5p overexpression in sEVs downregulates TLR4/ROS/MAPK pathway and inhibits NET formation. (**a**) Expression level of miR-17–5p, measured by RT-qPCR, in engineered hucMSCs. (**b**) Expression level of miR-17–5p, measured by RT-qPCR, in engineered sEVs. (**c**) Expression level of miR-17–5p, measured by RT-qPCR, in neutrophils after incubation with engineered sEVs for 24 h. (**d**) The protein level of TLR4 was detected in different groups by Western blot. (**e, f**) ROS level was examined by using DCFH-DA in neutrophils after incubation with engineered sEVs for 24 h. Scale bar, 200 μm. (**g, h**) Changes of MAPK pathway in neutrophils after incubation with engineered sEVs for 24 h were detected by Western blot. (**i, j**) Immunofluorescence analyses of NET formation in neutrophils treated with PMA (20 nM) or high concentration of glucose (35 mM) after incubation with engineered sEVs for 24 h. H3Cit, Green; MPO, red; DAPI, blue. Scale bar, 50 μm $^{**}p < 0.01$, $^{***}p < 0.001$.

Subsequently, TLR4 mRNA and protein expression level in neutrophils were found to be inhibited by overexpression of miR-17–5p, and knockdown of miR-17–5p led to elevation of TLR4 (Fig. 4i and j). Furthermore, Western blot analysis showed that both Normo-sEVs and Hypo-sEVs significantly downregulated TLR4 expression and Hypo-sEVs exhibited better efficacy (Fig. 4k). These findings demonstrate that TLR4 is a target gene of miR-17–5p.

Upon activation, TLR4 can trigger the release of reactive oxygen species (ROS) to control NET formation [32]. Increasing evidences have demonstrated that initiation of ROS burst in neutrophils played an important role in NETosis through regulating the phosphorylation of three branch cascade factors of mitogen-activated protein kinase (MAPK) pathway, including c-JUN N-terminal Kinase (JNK), extracellular regulated protein kinases (ERK) and p38 [33–36]. KEGG pathway enrichment analyses also revealed that MAPK signaling pathway might be regulated by miR-17–5p (Fig. 4l). Hence, we detected the ROS production and the expressions of p-JNK, p-ERK, and p-p38 in neutrophils after treatment with sEVs. The results showed that ROS level was significantly downregulated by Normo-sEVs or Hypo-sEVs, and Hypo-sEVs had better performance than Normo-sEVs (Fig. 4m). Likewise, both Normo-sEVs and Hypo-sEVs inhibited the phosphorylation of JNK, ERK and p38, and lower protein expression level was found in Hypo-sEVs group (Fig. 4n). These results suggest that downregulation of ROS-MAPK signaling pathway may be responsible for Hypo-sEVs induced inhibition on NET formation.

3.5. *miR-17–5p overexpression in sEVs downregulates TLR4/ROS/MAPK pathway and inhibits NET formation*

To determine the direct effect of miR-17–5p on NET formation, lentiviral was used to infect hucMSCs to build miR-17–5p overexpression (miR-17^{OE}), miR-17–5p knockdown (miR-17^{KD}) hucMSCs and the corresponding negative controls (miR-NC^{OE} and miR-NC^{KD}). The transfection efficiency was verified by RT-qPCR (Fig. 5a). Whereafter, sEVs were extracted from these engineered hucMSCs and named as miR-17^{OE}-sEVs, miR-NC^{OE}-sEVs, miR-17^{KD}-sEVs and miR-NC^{KD}-sEVs, respectively. NTA, TEM and Western blot were used to identify the characters of these engineered sEVs (Supplementary Figs. S3a–c), Additionally, expression level of miR-17–5p in sEVs was detected and the data revealed a similar trend of that in MSCs (Fig. 5b). Then we confirmed that these sEVs could also be taken up by neutrophils (Supplementary Fig. S3d). After treatment with these sEVs, miR-17–5p

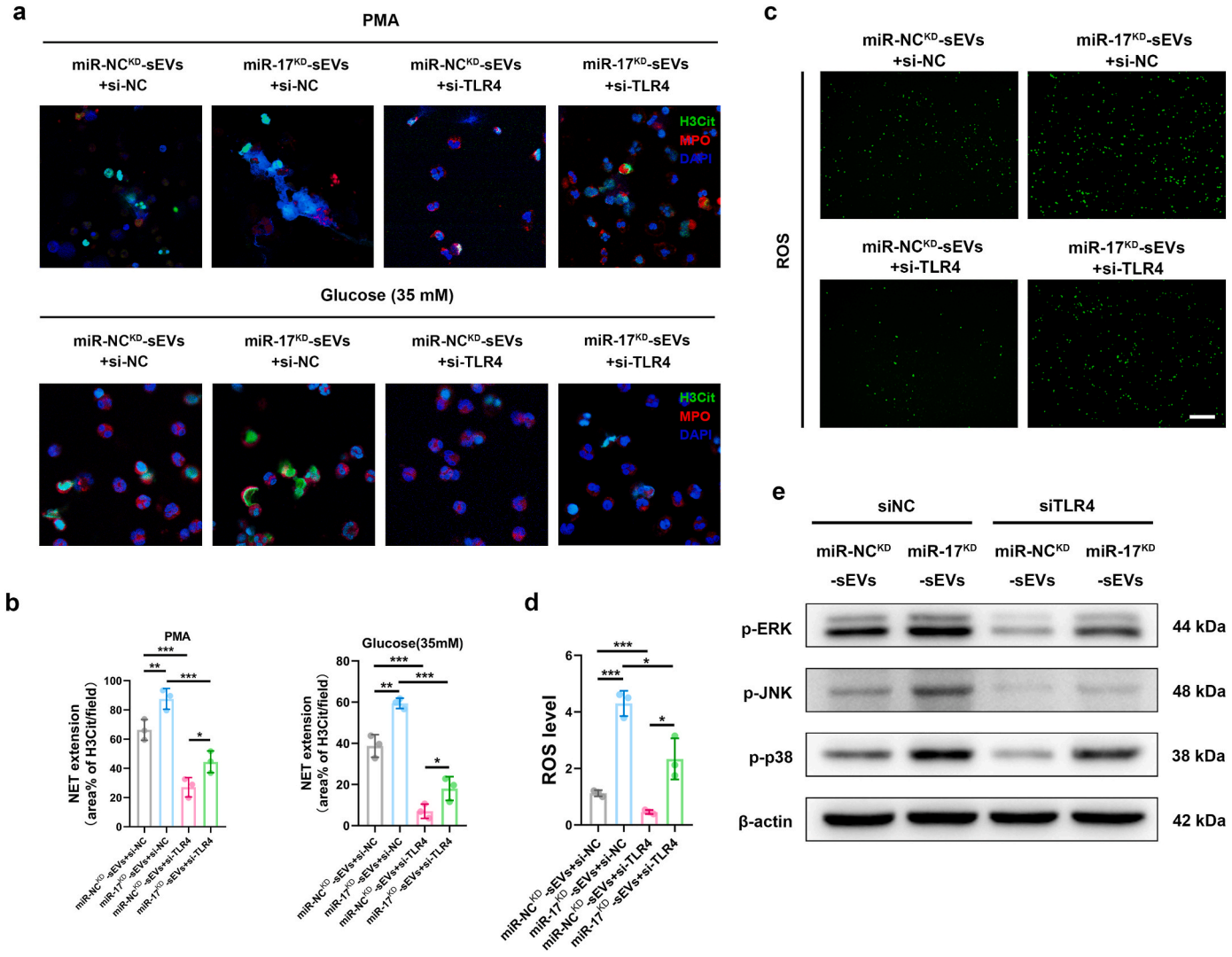

Fig. 6. Knockdown of TLR4 can partially rescue the effect of miR-17–5p on NET formation. (**a**) Representative confocal images of immunofluorescence of NET formation from different groups in rescue experiment. H3Cit, Green; MPO, red; DAPI, blue. Scale bar, 50 μm. (**b**) Quantification of the percentage of NETs areas. (**c, d**) ROS level from different groups in rescue experiment was measured by using DCFH-DA. Scale bar, 200 μm. (**e**) Western blot analysis of the expression level of MAPK signaling pathway in neutrophils under different treatments. *$p < 0.05$, **$p < 0.01$, ***$p < 0.001$.

expression level in neutrophils was significantly upregulated in miR-17^{OE}-sEVs group compared with miR-NC^{OE}-sEVs group. Addition of miR-17^{KD}-sEVs resulted in a significant decrease of miR-17–5p compared to that in miR-NC^{KD}-sEVs group (Fig. 5c). In addition, overexpression of miR-17–5p in neutrophils reduced the expression of TLR4 and opposite effect was found in miR-17^{KD}-sEVs group (Fig. 5d). Next, the production of ROS and the activity of MAPK signaling pathway were evaluated in neutrophils after administration of these engineered sEVs. We observed that overexpression of miR-17–5p significantly inhibited the ROS production and the expression of p-ERK, p-JNK and p-p38. While the production of ROS and the expression of p-ERK, p-JNK and p-p38 were elevated in miR-17^{KD}-sEVs group in comparison to miR-NC^{KD}-sEVs group (Fig. 5e–h). Consistent with the above findings, upregulation of miR-17–5p decreased NETosis induced by PMA or high concentration

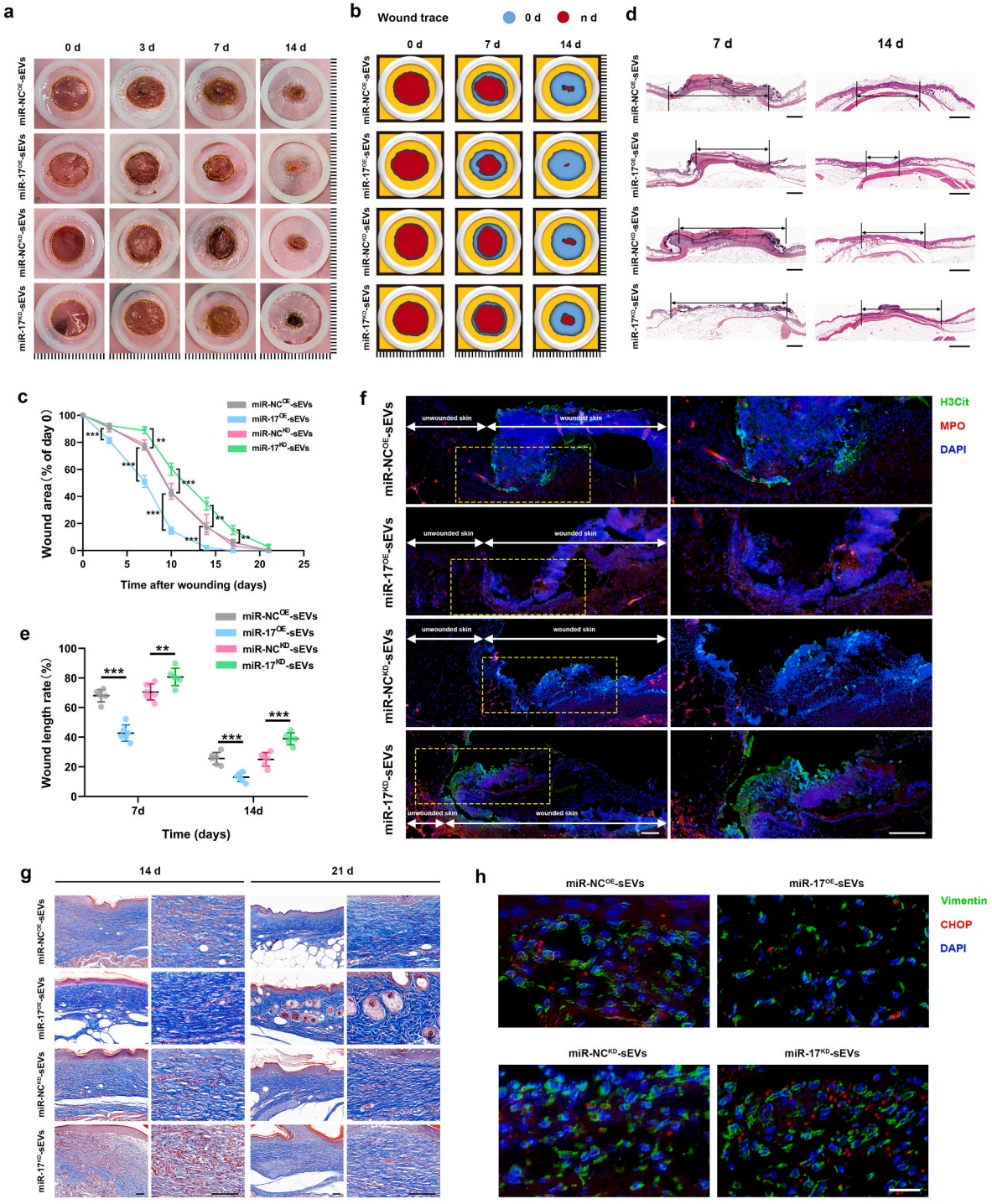

Fig. 7. MiR-17–5p in sEVs promotes diabetic wound healing via inhibiting NET-induced impairment on fibroblasts. (**a**) Gross view of diabetic wounds on days 0, 3, 7 and 14 post wounding with the administration of engineered sEVs. (**b**) Simulation plots of the wound closure areas. (**c**) Quantitative evaluation of the wound closure rate; n = 6. (**d**) Representative images of H&E staining of wound sections. Scale bar. 2 mm. (**e**) Quantitative analysis of the wound length rate; n = 6. (**f**) Representative confocal images of NETs areas in diabetic wounds on day 3 after injury. H3Cit, Green; MPO, red; DAPI, blue. Scale bar, 100 μm. (**g**) Representative images of Masson staining of wound sections. Scale bar, 100 μm. (**h**) Immunofluorescence analysis of ER stress marker, CHOP, in diabetic wound sections. Vimentin, Green; CHOP, red; DAPI, blue. Scale bar, 100 μm. ns: no significance, *$p < 0.05$, **$p < 0.01$, ***$p < 0.001$.

of glucose (Fig. 5i and j). These results indicate that sEVs miR-17–5p can simulate the effect of Hypo-sEVs on inhibiting ROS/MAPK activity and NET formation.

To further investigate the mechanism of sEVs miR-17–5p on inhibiting NET formation via targeting TLR4, we performed a rescue experiment. We found that knockdown of TLR4 could eliminate the effect of miR-17^{KD}-sEVs on NET formation (Fig. 6a and b and Supplementary Figs. S4a and b). We also observed that ROS production induced by miR-17^{KD}-sEVs was significantly downregulated by TLR4 silencing (Fig. 6c and d). Moreover, Western blot was performed to reveal that TLR4 siRNA could partially rescue the effect of sEVs miR-17–5p on regulation of MAPK signaling pathway (Fig. 6e). These results suggest that sEVs miR-17–5p can suppress the formation of NETs by downregulating TLR4/ROS/MAPK axis.

3.6. SEVs miR-17–5p promotes diabetic wound healing via inhibiting NET-induced impairment on fibroblasts

To better determine the role of sEVs miR-17–5p in the regulation of ER stress-induced NETs in vivo, miR-NC^{OE}-sEVs, miR-17^{OE}-sEVs, miR-NC^{KD}-sEVs or miR-17^{KD}-sEVs were injected intradermally at the diabetic wound edge every other day. Compared to control groups, almost all diabetic wounds in miR-17^{OE}-sEVs group were completely healed on day 14. In contrast, administration of miR-17^{KD}-sEVs eliminated the protective effects seen with miR-NC^{KD}-sEVs (Fig. 7a–e). Immunofluorescence staining showed that lower H3Cit expression was detected, presenting less NET formation, in the wounds treated with miR-17^{OE}-sEVs compared to the miR-NC^{OE}-sEVs group on day 3. While enhanced NETosis was found in miR-17^{KD}-sEVs group in comparison to miR-NC^{KD}-sEVs group (Fig. 7f). These results recapitulate our in vitro observations and further support the positive role of sEVs miR-17–5p in NET-induced delay of diabetic wound repair.

Additionally, Masson staining was performed to show that the wounds treated with miR-17^{OE}-sEVs had more extensive collagen deposition than that in the control group. The opposite result was found following miR-17^{KD}-sEVs administration (Fig. 7g). Furthermore, expression level of CHOP was analyzed in the wound tissues following sEVs treatment. As shown in Fig. 7h, decreased protein levels of CHOP was observed in vimentin $^{+}$ skin fibroblasts by treatment with miR-17^{OE}-sEVs, and utilization of miR-17^{KD}-sEVs obviously induced upregulated CHOP expression level compared to its control group. Collectively, these results indicate that miR-17–5p overexpression in sEVs can promote diabetic wound healing via improving the impaired function of fibroblasts caused by NET-induced ER stress.

4. Discussion

In the present study, we report a previously unrecognized NET-related mechanisms in diabetic wounds and develop a promising NET-targeting treatment based on Hypo-sEVs. Our works demonstrate that there are excessive NETs in diabetic wounds. High concentration of NETs impairs the fibroblast function by activating ER stress. Hypo-sEVs transferring miR-17–5p can block the formation of NETs and promote the diabetic wound healing by targeting TLR4/ROS/MAPK pathway (Supplementary Fig. S5). MiR-17–5p overexpression in engineered sEVs improves the impaired function of fibroblasts and decreases ER stress induced by NET formation, thereby enhancing diabetic wound healing.

In diabetic wound, NETs are abnormally accumulated. Several studies showed that excessive NETs released from neutrophils contribute to the pathogenesis of a growing number of diseases including cancer cell metastasis [37], autoimmune diseases [38], venous thromboembolism [39] and COVID-19 [40]. What's more, excessive NETs were also confirmed as a vital negative factor for regeneration of diabetic wounds [41]. However, these reports had not yet fully explained how NETs affected diabetic wound tissues. Several studies suggested that components of NETs, such as neutrophil elastase (NE), could lead to degradation of the wound matrix [42]. Moreover, an emerging role of NE was reported to induce ER stress by promoting ROS production in airway epithelial cells [43]. Extracellular histones and DNA, the main components of NETs, were also found to activate ER stress-mediated apoptosis via TLR receptors including TLR2, TLR4 and TLR9 [30,44]. It is well known that function of fibroblasts is essential for wound healing. In this study, our data revealed that high concentration of NETs significantly potentiated ER stress and apoptosis of fibroblasts in vitro and in vivo. The mechanisms of them might be explained by the effects of NET-derived DNA backbone which could activate ER stress through the aforementioned TLR receptors since the administration of DNase I could abolish the effect of NETs on ER stress. Furthermore, we also found that low concentration of NETs promoted the proliferation and migration of fibroblasts and also exhibited an inhibition on ER stress. A recent study showed that the transmembrane protein coiled-coil domain containing protein 25 (CCDC25) was confirmed as a NET-DNA receptor which can activate Integrin-linked kinase (ILK) [37]. Interestingly, ILK has been reported to activate PI3K/AKT pathway to promote cutaneous wound healing [45], and activation of PI3K/AKT signaling pathway could restrain ER stress and inhibit cell apoptosis [46,47]. These studies are consistent with our demonstration that low concentration of NETs (100 ng mL^{-1}) can inhibit ER stress. Similarly, a study by Stelvio et al. [5] revealed that low concentration of NETs increased HaCaT proliferation, while administration of higher concentration of NETs started to reduce keratinocytes proliferation. Hence, we hypothesize that activation of CCDC25/ILK/PI3K/AKT pathway may explain the role of low concentration of NETs on favoring fibroblast proliferation and migration. In summary, previous studies and present results together suggest that NETs are excessively accumulated under the diabetic microenvironment and are more prone to activate ER stress and apoptosis.

In diabetes, impaired wound healing is a major complication and seriously affects the health and prognosis of patients [48]. The emerging field of treating diseases with MSCs or MSC-derived sEVs is one of the most exciting frontiers in biomedical research. Recent studies have described that MSCs functioned in each phase of the diabetic wound repair process, such as enhancement of angiogenesis, improving granulation, facilitating re-epithelialization, and regulating inflammatory leukocytes-neutrophils and macrophages [49–51]. However, these positive effects of MSCs in the process seem to be mediated mainly by paracrine secretion. For example, sEVs derived from epidermal stem cells have been suggested to promote diabetic wound healing [52]. However, sEVs per se are not sufficient for rapid wound healing. Hence, modulating the compositions of sEVs possesses a better application prospect. Considering that hypoxia precondition can affect the secretion level and composition of sEVs [21], we pre-treated hucMSCs under hypoxic environment before extraction of sEVs. Here, we revealed that Hypo-sEVs secreted from MSCs played an essential role in inhibiting NET formation. Compared with Normo-sEVs, Hypo-sEVs exhibited increased abilities to promote wound healing in diabetic mice. MiRNAs are short RNA molecules that play vital role in multiple biological processes by regulating stability or translational efficiency of target genes [53]. When miRNAs are secreted into sEVs, the biological membrane of sEVs can protect the miRNAs from degradation by the external environment [54]. Previous studies demonstrated that miRNAs contained in sEVs had the potential to exert therapeutic effects. A significant upregulation of miR-20b-5p was found in sEVs from diabetes and knocking out miR-20b-5p significantly enhanced diabetic wound healing [55]. Our prior studies have indicated that miR-17–5p was upregulated in hucMSC-sEVs and overexpression of miR-17–5p accelerated diabetic wound healing partially through triggering angiogenesis [17]. Interestingly, higher abundance of miR-17–5p in Hypo-sEVs and recipient neutrophils was observed compared to that in Normo-sEVs, indicating that Hypo-sEVs miR-17–5p could be a new approach for treating diabetic wounds.

By using bioinformatic tools, combined with the overexpression of miR-17–5p in Hypo-sEVs and recipient neutrophils, we found that

MAPK signaling pathway was a downstream of miR-17–5p. Several studies revealed that various TLRs, including TLR2, TLR4, TLR6, TLR7, TLR8 and TLR9, could regulate NET formation [18,32,56–59]. The toll-like receptor 4 (TLR4), verified as a potential target of miR-17–5p based on database prediction and dual-luciferase reporter gene assay, was selected for further study. When miR-17–5p was overexpressed, mRNA and protein level of TLR4 were significantly decreased in neutrophils. A study showed that TLR4 contributed to the formation of NETs through regulating ROS production in neutrophils [32], and a key upstream regulatory channel of NET formation is MAPK signaling pathway, which is primarily orchestrated by ROS from NADPH oxidase [60]. Hence, the present results highlighted the role of miR-17–5p in NET activation. In addition, we observed downregulated ROS production and phosphorylation level of MAPK pathway under administration of Hypo-sEVs, suggesting that miR-17–5p was involved in the inactivation of MAPK pathway. Subsequently, we found that knockdown of miR-17–5p in MSC-sEVs abolished the effect of sEVs in inhibiting ROS/MAPK axis and NET formation. By utilizing a series of rescue experiments, our results revealed that silencing of TLR4 reversed the negative effect of miR-17–5p knockdown in sEVs. Collectively, these data indicate that Hypo-sEVs derived from hucMSCs effectively suppress NET formation partially through miR-17-5p-mediated suppressing of TLR4/ROS/MAPK pathway, thus improving diabetic wound healing.

5. Conclusion

In summary, our findings indicate that sEVs from hypoxic hucMSCs can suppress the formation of NETs in diabetic wounds by delivering miR-17–5p, and this effect occurs through targeting TLR4 and inhibition of MAPK signaling pathway. In addition, ER stress activation is revealed to play the predominant role in NET-induced delay of diabetic wound healing. Our work not only refines the understanding of NETs in diabetes, but also provides a promising strategy for the treatment of diabetic wound.

Ethics approval and consent to participate

Animals

The animal studies were approved by the Animal Research Committee of PLA General Hospital in Beijing, China. All mice were fed under standard laboratory condition free of specific pathogens.

CRediT authorship contribution statement

Ziqiang Chu: Formal analysis, Conceptualization, Investigation, Methodology, Writing - original draft. **Haihong Li:** Funding acquisition, Supervision, Writing - review & editing. **Xiaobing Fu:** Funding acquisition, Supervision, Writing - review & editing. **Cuiping Zhang:** Funding acquisition, Supervision, Writing - review & editing.

Declaration of competing interest

The authors declare that they have no known competing financial interests or personal relationships that could have appeared to influence the work reported in this paper.

Acknowledgements

We thank BioRender.com for the drawing of graphics. This work was supported by National Natural Science Foundation of China (82172211, 92268206, 22205260, 81830064, 82172231), National Key Research and Development Programs of China (2022YFA1104303), CAMS Innovation Fund for Medical Sciences (CIFMS, 2019-I2M-5–059), Military Medical Research and Development Projects (AWS17J005, 2019–126) and Military Medical Science and Technology Youth Training Program (21QNPY128).

Appendix A. Supplementary data

Supplementary data to this article can be found online at https://doi.org/10.1016/j.bioactmat.2023.04.007.

References

[1] R. van Wilpe, A.H. Hulst, S.E. Siegelaar, et al., Type 1 and other types of diabetes mellitus in the perioperative period. What the anaesthetist should know, J. Clin. Anesth. 84 (2023), 111012, https://doi.org/10.1016/j.jclinane.2022.111012.
[2] D.G. Armstrong, A.J.M. Boulton, S.A. Bus, Diabetic foot ulcers and their recurrence, N. Engl. J. Med. 376 (24) (2017) 2367–2375, https://doi.org/10.1056/NEJMra1615439.
[3] J. Wang, Neutrophils in tissue injury and repair, Cell Tissue Res. 371 (3) (2018) 531–539, https://doi.org/10.1007/s00441-017-2785-7.
[4] S. Boeltz, P. Amini, H.-J. Anders, et al., To NET or not to NET:current opinions and state of the science regarding the formation of neutrophil extracellular traps, Cell Death Differ. 26 (3) (2019) 395–408, https://doi.org/10.1038/s41418-018-0261-x.
[5] S. Tonello, M. Rizzi, M. Migliario, et al., Low concentrations of neutrophil extracellular traps induce proliferation in human keratinocytes via NF-kB activation, J. Dermatol. Sci. 88 (1) (2017) 110–116, https://doi.org/10.1016/j.jdermsci.2017.05.010.
[6] S.L. Wong, M. Demers, K. Martinod, et al., Diabetes primes neutrophils to undergo NETosis, which impairs wound healing, Nat. Med. 21 (7) (2015) 815–819, https://doi.org/10.1038/nm.3887.
[7] Y. Liu, C. Li, Z. Feng, et al., Advances in the preparation of nanofiber dressings by electrospinning for promoting diabetic wound healing, Biomolecules 12 (12) (2022), https://doi.org/10.3390/biom12121727.
[8] X. Qi, X. Tong, S. You, et al., Mild hyperthermia-assisted ROS scavenging hydrogels achieve diabetic wound healing, ACS Macro Lett. 11 (7) (2022) 861–867, https://doi.org/10.1021/acsmacrolett.2c00290.
[9] X.L. Qi, Y.J. Xiang, E. Cai, et al., All-in-one: harnessing multifunctional injectable natural hydrogels for ordered therapy of bacteria-infected diabetic wounds, Chem. Eng. J. 439 (2022), https://doi.org/10.1016/j.cej.2022.135691.
[10] Y. An, S. Lin, X. Tan, et al., Exosomes from adipose-derived stem cells and application to skin wound healing, Cell Prolif. 54 (3) (2021), e12993, https://doi.org/10.1111/cpr.12993.
[11] L. Barkholt, E. Flory, V. Jekerle, et al., Risk of tumorigenicity in mesenchymal stromal cell-based therapies–bridging scientific observations and regulatory viewpoints, Cytotherapy 15 (7) (2013) 753–759, https://doi.org/10.1016/j.jcyt.2013.03.005.
[12] D. Furlani, M. Ugurlucan, L. Ong, et al., Is the intravascular administration of mesenchymal stem cells safe? Mesenchymal stem cells and intravital microscopy, Microvasc. Res. 77 (3) (2009) 370–376, https://doi.org/10.1016/j.mvr.2009.02.001.
[13] T.N. Lamichhane, S. Sokic, J.S. Schardt, et al., Emerging roles for extracellular vesicles in tissue engineering and regenerative medicine, Tissue Eng. B Rev. 21 (1) (2015) 45–54, https://doi.org/10.1089/ten.TEB.2014.0300.
[14] Q. Zeng, Y. Qian, Y. Huang, et al., Polydopamine nanoparticle-dotted food gum hydrogel with excellent antibacterial activity and rapid shape adaptability for accelerated bacteria-infected wound healing, Bioact. Mater. 6 (9) (2021) 2647–2657, https://doi.org/10.1016/j.bioactmat.2021.01.035.
[15] T. Su, M. Zhang, Q. Zeng, et al., Mussel-inspired agarose hydrogel scaffolds for skin tissue engineering, Bioact. Mater. 6 (3) (2021) 579–588, https://doi.org/10.1016/j.bioactmat.2020.09.004.
[16] H. Abbaszadeh, F. Ghorbani, M. Derakhshani, et al., Human umbilical cord mesenchymal stem cell-derived extracellular vesicles: a novel therapeutic paradigm, J. Cell. Physiol. 235 (2) (2020) 706–717, https://doi.org/10.1002/jcp.29004.
[17] Q. Wei, Y. Wang, K. Ma, et al., Extracellular vesicles from human umbilical cord mesenchymal stem cells facilitate diabetic wound healing through MiR-17-5p-mediated enhancement of angiogenesis, Stem Cell Rev Rep 18 (3) (2022) 1025–1040, https://doi.org/10.1007/s12015-021-10176-0.
[18] D. Awasthi, S. Nagarkoti, A. Kumar, et al., Oxidized LDL induced extracellular trap formation in human neutrophils via TLR-PKC-IRAK-MAPK and NADPH-oxidase activation, Free Radic. Biol. Med. 93 (2016) 190–203, https://doi.org/10.1016/j.freeradbiomed.2016.01.004.
[19] L. Chen, L. Hu, Q. Li, et al., Exosome-encapsulated miR-505 from ox-LDL-treated vascular endothelial cells aggravates atherosclerosis by inducing NET formation, Acta Biochim. Biophys. Sin. 51 (12) (2019) 1233–1241, https://doi.org/10.1093/abbs/gmz123.
[20] H. Gao, X. Wang, C. Lin, et al., Exosomal MALAT1 derived from ox-LDL-treated endothelial cells induce neutrophil extracellular traps to aggravate atherosclerosis, Biol. Chem. 401 (3) (2020) 367–376, https://doi.org/10.1515/hsz-2019-0219.
[21] S. Yaghoubi, H. Najminejad, M. Dabaghian, et al., How hypoxia regulate exosomes in ischemic diseases and cancer microenvironment? IUBMB Life 72 (7) (2020) 1286–1305, https://doi.org/10.1002/iub.2275.
[22] J. Wang, H. Wu, Y. Peng, et al., Hypoxia adipose stem cell-derived exosomes promote high-quality healing of diabetic wound involves activation of PI3K/Akt pathways, J. Nanobiotechnol. 19 (1) (2021) 202, https://doi.org/10.1186/s12951-021-00942-0.

[23] B. Koch, A. Geßner, S. Farmand, et al., Effects of hypoxia on RNA cargo in extracellular vesicles from human adipose-derived stromal/stem cells, Int. J. Mol. Sci. 23 (13) (2022), https://doi.org/10.3390/ijms23137384.
[24] Z.-M. Zhou, J.-P. Bao, X. Peng, et al., Small extracellular vesicles from hypoxic mesenchymal stem cells alleviate intervertebral disc degeneration by delivering miR-17-5p, Acta Biomater. 140 (2022) 641–658, https://doi.org/10.1016/j.actbio.2021.11.044.
[25] S. Najmeh, J. Cools-Lartigue, B. Giannias, et al., Simplified human neutrophil extracellular traps (NETs) isolation and handling, J. Vis. Exp. 98 (2015), https://doi.org/10.3791/52687.
[26] J. He, Z. Chu, W. Lai, et al., Circular RNA circHERC4 as a novel oncogenic driver to promote tumor metastasis via the miR-556-5p/CTBP2/E-cadherin axis in colorectal cancer, J. Hematol. Oncol. 14 (1) (2021) 194, https://doi.org/10.1186/s13045-021-01210-2.
[27] Y. Wang, Z. Cao, Q. Wei, et al., VH298-loaded extracellular vesicles released from gelatin methacryloyl hydrogel facilitate diabetic wound healing by HIF-1α-mediated enhancement of angiogenesis, Acta Biomater. 147 (2022) 342–355, https://doi.org/10.1016/j.actbio.2022.05.018.
[28] Y. Xiao, M. Cong, J. Li, et al., Cathepsin C promotes breast cancer lung metastasis by modulating neutrophil infiltration and neutrophil extracellular trap formation, Cancer Cell 39 (3) (2021), https://doi.org/10.1016/j.ccell.2020.12.012.
[29] A. Hawez, A. Al-Haidari, R. Madhi, et al., MiR-155 regulates PAD4-dependent formation of neutrophil extracellular traps, Front. Immunol. 10 (2019) 2462, https://doi.org/10.3389/fimmu.2019.02462.
[30] S. Sun, Z. Duan, X. Wang, et al., Neutrophil extracellular traps impair intestinal barrier functions in sepsis by regulating TLR9-mediated endoplasmic reticulum stress pathway, Cell Death Dis. 12 (6) (2021) 606, https://doi.org/10.1038/s41419-021-03896-1.
[31] G. Tumurkhuu, D.E. Laguna, R.E. Moore, et al., Neutrophils contribute to ER stress in lung epithelial cells in the pristane-induced diffuse alveolar hemorrhage mouse model, Front. Immunol. 13 (2022), 790043, https://doi.org/10.3389/fimmu.2022.790043.
[32] Y. Dong, C. Jin, Z. Ding, et al., TLR4 regulates ROS and autophagy to control neutrophil extracellular traps formation against Streptococcus pneumoniae in acute otitis media, Pediatr. Res. 89 (4) (2021) 785–794, https://doi.org/10.1038/s41390-020-0964-9.
[33] M. Ravindran, M.A. Khan, N. Palaniyar, Neutrophil extracellular trap formation: physiology, pathology, and pharmacology, Biomolecules 9 (8) (2019), https://doi.org/10.3390/biom9080365.
[34] I.J. Chicca, M.R. Milward, I.L.C. Chapple, et al., Development and application of high-content biological screening for modulators of NET production, Front. Immunol. 9 (2018) 337, https://doi.org/10.3389/fimmu.2018.00337.
[35] Z.-R. Xu, J.-Y. Li, X.-W. Dong, et al., Apple polyphenols decrease atherosclerosis and hepatic steatosis in ApoE-/- mice through the ROS/MAPK/NF-κB pathway, Nutrients 7 (8) (2015) 7085–7105, https://doi.org/10.3390/nu7085324.
[36] Z. Yang, S. Wang, K. Yin, et al., MiR-1696/GPx 3 axis is involved in oxidative stress mediated neutrophil extracellular traps inhibition in chicken neutrophils, J. Cell. Physiol. 236 (5) (2021) 3688–3699, https://doi.org/10.1002/jcp.30105.
[37] L. Yang, Q. Liu, X. Zhang, et al., DNA of neutrophil extracellular traps promotes cancer metastasis via CCDC25, Nature 583 (7814) (2020) 133–138, https://doi.org/10.1038/s41586-020-2394-6.
[38] M.J. Podolska, A. Mahajan, J. Knopf, et al., Autoimmune, rheumatic, chronic inflammatory diseases: neutrophil extracellular traps on parade, Autoimmunity 51 (6) (2018) 281–287, https://doi.org/10.1080/08916934.2018.1519804.
[39] C. Thålin, Y. Hisada, S. Lundström, et al., Neutrophil extracellular traps: villains and targets in arterial, venous, and cancer-associated thrombosis, Arterioscler. Thromb. Vasc. Biol. 39 (9) (2019) 1724–1738, https://doi.org/10.1161/ATVBAHA.119.312463.
[40] B.J. Barnes, J.M. Adrover, A. Baxter-Stoltzfus, et al., Targeting potential drivers of COVID-19: neutrophil extracellular traps, J. Exp. Med. 217 (6) (2020), https://doi.org/10.1084/jem.20200652.
[41] R.J. Roth Flach, M.P. Czech, NETs and traps delay wound healing in diabetes, Trends Endocrinol. Metabol. 26 (9) (2015) 451–452, https://doi.org/10.1016/j.tem.2015.07.004.
[42] H. Capella-Monsonís, M.A. Tilbury, J.G. Wall, et al., Porcine mesothelium matrix as a biomaterial for wound healing applications, Mater Today Bio 7 (2020), 100057, https://doi.org/10.1016/j.mtbio.2020.100057.
[43] X. Xu, Q. Li, L. Li, et al., Endoplasmic reticulum stress/XBP1 promotes airway mucin secretion under the influence of neutrophil elastase, Int. J. Mol. Med. 47 (5) (2021), https://doi.org/10.3892/ijmm.2021.4914.
[44] T. Quillard, H.A. Araújo, G. Franck, et al., TLR2 and neutrophils potentiate endothelial stress, apoptosis and detachment: implications for superficial erosion, Eur. Heart J. 36 (22) (2015) 1394–1404, https://doi.org/10.1093/eurheartj/ehv044.
[45] G. Li, Y.-Y. Li, J.-E. Sun, et al., ILK-PI3K/AKT pathway participates in cutaneous wound contraction by regulating fibroblast migration and differentiation to myofibroblast, Lab. Invest. 96 (7) (2016) 741–751, https://doi.org/10.1038/labinvest.2016.48.
[46] S. Kim, C.-H. Woo, Laminar flow inhibits ER stress-induced endothelial apoptosis through PI3K/Akt-Dependent signaling pathway, Mol. Cell. 41 (11) (2018) 964–970, https://doi.org/10.14348/molcells.2018.0111.
[47] C.-Y. Huang, J.-S. Deng, W.-C. Huang, et al., Attenuation of lipopolysaccharide-induced acute lung injury by hispolon in mice, through regulating the TLR4/PI3K/Akt/mTOR and keap 1/nrf 2/HO-1 pathways, and suppressing oxidative stress-mediated ER stress-induced apoptosis and autophagy, Nutrients 12 (6) (2020), https://doi.org/10.3390/nu12061742.
[48] S. Patel, S. Srivastava, M.R. Singh, et al., Mechanistic insight into diabetic wounds: pathogenesis, molecular targets and treatment strategies to pace wound healing, Biomed. Pharmacother. 112 (2019), 108615, https://doi.org/10.1016/j.biopha.2019.108615.
[49] J. Yan, J. Liang, Y. Cao, et al., Efficacy of topical and systemic transplantation of mesenchymal stem cells in a rat model of diabetic ischemic wounds, Stem Cell Res. Ther. 12 (1) (2021) 220, https://doi.org/10.1186/s13287-021-02288-8.
[50] C.S. Pak, C.Y. Heo, J. Shin, et al., Effects of a catechol-functionalized hyaluronic acid patch combined with human adipose-derived stem cells in diabetic wound healing, Int. J. Mol. Sci. 22 (5) (2021), https://doi.org/10.3390/ijms22052632.
[51] Y. Cao, X. Gang, C. Sun, et al., Mesenchymal stem cells improve healing of diabetic foot ulcer, J. Diabetes Res. 2017 (2017), 9328347, https://doi.org/10.1155/2017/9328347.
[52] P. Wang, G. Theocharidis, I.S. Vlachos, et al., Exosomes derived from epidermal stem cells improve diabetic wound healing, J. Invest. Dermatol. 142 (9) (2022), https://doi.org/10.1016/j.jid.2022.01.030.
[53] M.A. Mori, R.G. Ludwig, R. Garcia-Martin, et al., Extracellular miRNAs: from biomarkers to mediators of physiology and disease, Cell Metabol. 30 (4) (2019) 656–673, https://doi.org/10.1016/j.cmet.2019.07.011.
[54] C. Miao, X. Wang, W. Zhou, et al., The emerging roles of exosomes in autoimmune diseases, with special emphasis on microRNAs in exosomes, Pharmacol. Res. 169 (2021), 105680, https://doi.org/10.1016/j.phrs.2021.105680.
[55] Y. Xiong, L. Chen, C. Yan, et al., Circulating exosomal miR-20b-5p inhibition restores Wnt9b signaling and reverses diabetes-associated impaired wound healing, Small 16 (3) (2020), e1904044, https://doi.org/10.1002/smll.201904044.
[56] J.S. Hook, P.A. Patel, A. O'Malley, et al., Lipoproteins from drive neutrophil extracellular trap formation in a TLR2/1- and PAD-dependent manner, J. Immunol. 207 (3) (2021) 966–973, https://doi.org/10.4049/jimmunol.2100283.
[57] C. Lood, S. Arve, J. Ledbetter, et al., TLR7/8 activation in neutrophils impairs immune complex phagocytosis through shedding of FcgRIIA, J. Exp. Med. 214 (7) (2017) 2103–2119, https://doi.org/10.1084/jem.20161512.
[58] B. Mallavia, F. Liu, E. Lefrançais, et al., Mitochondrial DNA stimulates TLR9-dependent neutrophil extracellular trap formation in primary graft dysfunction, Am. J. Respir. Cell Mol. Biol. 62 (3) (2020) 364–372, https://doi.org/10.1165/rcmb.2019-0140OC.
[59] K. Zhang, N. Jiang, X. Sang, et al., Lipophosphoglycan induces the formation of neutrophil extracellular traps and reactive oxygen species burst toll-like receptor 2, toll-like receptor 4, and c-jun N-terminal kinase activation, Front. Microbiol. 12 (2021), 713531, https://doi.org/10.3389/fmicb.2021.713531.
[60] F. Ma, X. Chang, G. Wang, et al., Serotype 2 stimulates neutrophil extracellular traps formation via activation of p38 MAPK and ERK1/2, Front. Immunol. 9 (2018) 2854, https://doi.org/10.3389/fimmu.2018.02854.